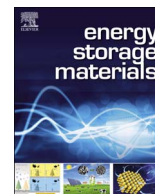




ELSEVIER

Contents lists available at ScienceDirect

Energy Storage Materials

journal homepage: www.elsevier.com/locate/ensm

Uncovering the Cu-driven electrochemical mechanism of transition metal chalcogenides based electrodes

Qidong Li^{a,c}, Qiulong Wei^{a,b}, Qinyou An^a, Lei Huang^a, Wen Luo^a, Xiaoji Ren^a, Kwadwo Asare Owusu^a, Feng Dong^a, Li Li^a, Peng Zhou^a, Liqiang Mai^{a,*}, Qingjie Zhang^a, Khalil Amine^{c,d,e}, Jun Lu^{c,*}

^a State Key Laboratory of Advanced Technology for Materials Synthesis and Processing, International School of Materials Science and Engineering, Wuhan University of Technology, Wuhan 430070, Hubei, China

^b Department of Materials Science and Engineering, University of California Los Angeles, Los Angeles, CA 90095-1595, USA

^c Chemical Sciences and Engineering Division, Argonne National Laboratory, Argonne, IL 60439, USA

^d Institute for Research and Medical Consultations, Imam Abdulrahman Bin Faisal University, Dammam, 34212 Saudi Arabia

^e Material Science and Engineering, Stanford University, Stanford, CA 94305 USA

ARTICLE INFO

Keywords:

Transition-metal chalcogenides
Sodium-ion batteries
Cu-driven conversion mechanism
Current collector
Sulfur-based battery

ABSTRACT

Transition-metal chalcogenides (TMCs) have emerged as attractive anode materials for rechargeable batteries due to their excellent performance and abundant resources. Here, for the first time, we disclose a unique copper (Cu)-driven conversion process in TMC-based battery systems that involves classic Cu current collector and is considered to be an “activation process”. According to state-of-the-art characterization techniques, Cu was evidenced to gradually replace the transition-metal elements in TMCs to be the active material during cycling. Based on this unique Cu-driven conversion mechanism, we used a facile method to design a new type of sulfur-based battery that presents excellent performance: a reversible capacity of 1.045 mAh cm⁻² after 700 cycles at 2 A g⁻¹, and a good rate capability up to a capacity of 0.33 mAh cm⁻² at 20 A g⁻¹. With respect to the large family of TMC compounds, this study introduces a new direction for the design of high-performance energy storage systems.

1. Introduction

Currently, environmental consequences such as global warming and pollution, which are generated by the consumption of fossil fuels, have increased the demand for renewable and sustainable energy resources. Solar and wind systems have shown considerable promise as large-scale clean-energy systems as a result of numerous breakthroughs in the last few years [1,2]. The utilization of electricity generated from such intermittent energy sources requires efficient energy storage systems. Lithium-ion batteries (LIBs) are one of the most popular energy storage techniques because of their merits, such as high energy density and no memory effect [3]. However, the increasing utilization of limited lithium resources in energy storage applications has pushed up the price of lithium compounds, making it difficult for LIBs to meet the demands of the proposed low-cost, large-scale energy storage applications. Owing to the electrochemical similarities between Li and Na, sodium-ion batteries (SIBs) have shown their great potential in electrochemical energy storage owing to the low cost

and abundance of sodium resources [4]. However, the larger size of Na⁺ compared to Li⁺ makes finding an appropriate host material more challenging. Therefore, additional exploration of new sodium storage systems is urgently needed [4–7].

As an important component of rechargeable batteries, anode materials have long been a hot topic for researchers. Among the three typical anode materials, conversion-type materials (such as transition-metal oxides and transition-metal chalcogenides (TMCs)) have drawn wide attention because of their high capacity and the wide distribution of raw resources. Recently, TMCs (MoS₂, FeS₂, FeSe₂, CoSe₂, etc.) have been reported with decent sodium storage performance in terms of long-term cyclability and high rate capability [8–14]. However, despite their impressive performance, these TMCs feature a common characteristic: the charge/discharge curves (potential plateau) of the TMCs change dramatically during cycling process, and this has been attributed to an activation process in previous reports [10,11]. Without further clarification, the assumed “activation process” seems to be a panacea of this abnormal voltage evolution, with researchers remaining

* Corresponding authors.

E-mail addresses: mlq518@whut.edu.cn (L. Mai), junlu@anl.gov (J. Lu).

<https://doi.org/10.1016/j.ensm.2018.07.002>

Received 19 April 2018; Received in revised form 20 June 2018; Accepted 1 July 2018
2405-8297/ © 2018 Published by Elsevier B.V.

unaware of some of the underlying electrochemical processes involved in TMCs anodes.

In this work, we demonstrate that the “activation process” in TMCs for sodium storage is actually a copper (Cu)-driven conversion process. During cycling, Cu replaces the transition-metal elements in the TMC materials to be the active material. By cleverly using this Cu-driven conversion mechanism, we developed a new type of sulfur-based battery that is mainly composed of three simple components: sublimed sulfur, Cu foil, and sodium anode. In contrast to traditional RT sodium-sulfur batteries, this new type of battery possesses a new reaction mechanism in which the Cu current collector plays a vital role, and enables a high reversible capacity of $1.045 \text{ mAh cm}^{-2}$ to be reached after 700 cycles at 2 A g^{-1} with little capacity loss and a high Coulombic efficiency of $\sim 100\%$. These outstanding properties along with the low-cost manufacturing technique, make this new type of sulfur-based battery a promising candidate for large-scale energy storage systems. Furthermore, we propose a new principle of choosing the desired current collector for an energy storage system, as this approach will guide the design of future electrode materials and advance fundamental studies of both lithium and sodium storage.

2. Materials and methods

2.1. Experimental methods

2.1.1. Preparation of FeS_2

FeS_2 (pyrite) was purchased and grounded to fine powder.

2.1.2. Preparation of NiS_2

18 ml of ethylenediamine and 18 ml of glycol were mixed for 10 mins, then 1 mmol of $\text{NiCl}_2 \cdot 6\text{H}_2\text{O}$ and 4 mmol of sulfur powder were added into the above solution. After stirring for another 30 mins, the suspension was transferred into a 50 ml Teflon-lined sealed autoclave and maintained at 180°C for 12 h. Finally, the autoclave was cooled down to room temperature naturally. The black precipitates were collected and washed with distilled water and absolute alcohol several times by centrifugation. Then the products were dried under vacuum at 80°C overnight.

2.1.3. Preparation of CoSe_2

Two solutions were first prepared. Solution A was prepared from 0.32 g of selenium powder dissolved in 30 ml of NaOH (4 g) aqueous solution. Solution B was prepared from 0.48 g of $\text{CoCl}_2 \cdot 6\text{H}_2\text{O}$ dissolved in 10 ml of 0.25 M EDTA solution. Then, the two solutions were poured into a 50 ml Teflon-lined sealed autoclave and maintained at 140°C for 36 h. The obtained product was collected and washed with dilute acid and distilled water, and then dried under vacuum at 80°C overnight.

2.1.4. Preparation of FeSe_2

2 mmol of $\text{Fe}(\text{NH}_4)_2(\text{SO}_4)_2 \cdot 6\text{H}_2\text{O}$, 4 mmol of Se powder, and 20.8 mmol of citric acid were added into 44 ml of distilled water, and then 16 ml of hydrazine hydrate was added drop-wise into the mixture. After vigorous stirring and sonication for 30 mins, the suspension was transferred into a 100 ml Teflon-lined sealed autoclave to heat at 180°C for 12 h. The as-prepared product was washed thoroughly with distilled water and absolute ethanol, and then dried under vacuum at 80°C overnight.

2.2. Material characterization

Field emission scanning electron microscopy images were performed by a JEOL-7100F microscope. XRD and *in-situ* XRD patterns of the samples were obtained with a D8 Advance X-ray diffractometer, using Cu-K α radiation ($\lambda = 1.5418 \text{ \AA}$). 200 nm Cu was deposited on Be by physical vapor deposition. TEM and HRTEM images were collected with a JSM-2010 microscope. Element mapping was tested by using an EDX-GENESIS 60S spectrometer.

2.3. Preparation of electrodes

The working electrodes were prepared by mixing 80 wt% active material, 15 wt% acetylene black and 5 wt% carboxyl methyl cellulose (CMC) binder. The slurry was cast onto Cu and Ti foil by using a doctor blade and dried in a vacuum oven at 80°C for 8 h, respectively. The mass loading of active materials was $0.8\text{--}5.0 \text{ mg cm}^{-2}$. Specially, for S electrode, it should be dried in a vacuum oven at room-temperature and then transferred into a freezer immediately after casting onto Cu foil. The reason is that S can react with Cu easily even at room-temperature.

2.4. Electrochemical performance test

The electrochemical properties were characterized in 2016 coin cells with sodium foils as the counter electrode. Ether-based solution (1 M NaCF_3SO_3 in diethyleneglycol dimethylether (DEGDME)) is used as the electrolyte. A composite membrane consisting of glass fiber/Celgard 2400/glass fiber (Fig. S11) is used as the membrane to prevent overcharge. Due to the large porosity of the glass fiber, the sodium-dendrites will penetrate the membrane resulting in the over-charging of the battery, as shown in Fig. S11b. The composite membrane prevents the over-charging completely, since the sodium-dendrites cannot penetrate the Celgard 2400 due to its low porosity and plate on the interface between the glass fiber and the Celgard 2400 (Fig. S11c). Galvanostatic charge/discharge measurements were performed using a multichannel battery testing system (LAND CT2001A). Cyclic voltammetry (CV) was collected with an Autolab potentiostat/galvanostat at room temperature.

3. Results and discussion

Here, we focus on studying the properties of four typical TMCs. FeSe_2 , CoSe_2 and NiS_2 were prepared as described in previous literatures [10,15,16], and FeS_2 (pyrite) was purchased. Scanning electron microscopy (SEM) images, digital photo, and X-ray diffraction (XRD) patterns of the TMCs are shown in Fig. S1. The XRD patterns are consistent with previous reports, and no impurity peaks are detected in any of the samples, indicating that all four samples were highly pure.

Coin-cells were used to examine the electrochemical performance of the four samples. All samples were fabricated into electrodes using the following previously reported method. The electrodes were prepared by mixing the electroactive materials, acetylene black, and carboxyl methyl cellulose at a weight ratio of 80:15:5. Then the slurry was cast onto Cu foil and dried in a vacuum oven at 80°C for 12 h (see the Supplementary information for further details). All electrochemical tests were performed by assembling and testing coin 2016-type half cells. An ether-based solution (1 M NaCF_3SO_3 in diethyleneglycol dimethylether (DEGDME)) was used as the electrolyte. All cells were tested between 0.2 and 3.0 V at a current density of 1 A g^{-1} . Notably, the discharge/charge plateaus of the four samples vary continuously during the cycling process, as mentioned above (Fig. 1a-d). However, this phenomenon is abnormal. For battery systems, the discharge/charge plateaus are generated from the redox reaction of the redox couple [17]. The potential shift is probably due to a change of redox couple.

The structure and contact interfaces of the working electrode in SIBs during the cycling process are illustrated in Fig. 1e (taking FeS_2 as an example). The basic principle when choosing a current collector is that the electrolyte should not react with the current collector. For a long time, Cu has been considered to be an ideal current collector for anode materials. FeS_2 converts into a compound consisting of Fe and Na_2S when the battery is discharged to a low potential (0.2 V here) [18], as depicted in Eq. 1:



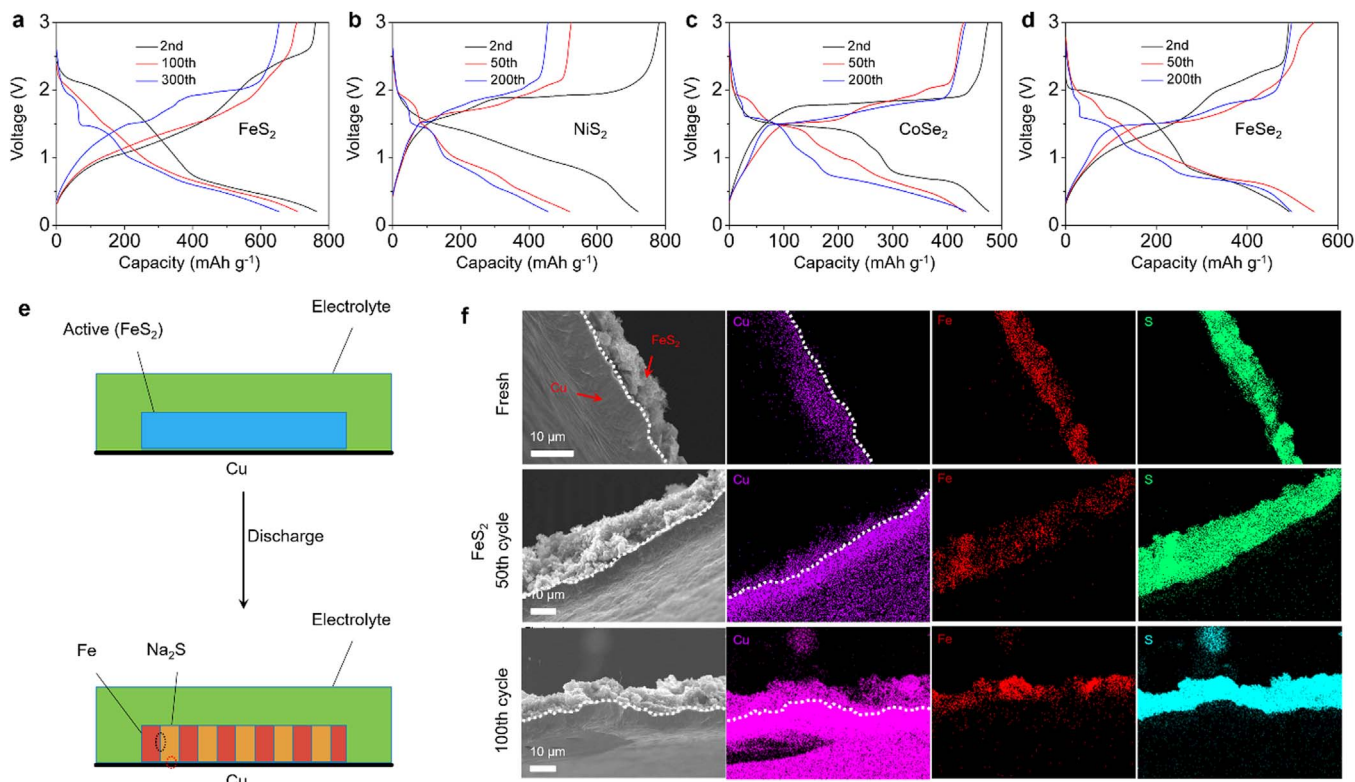
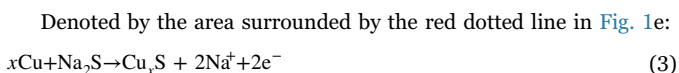
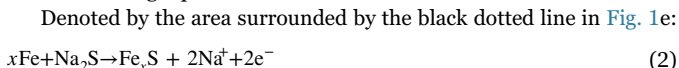


Fig. 1. The discharge/charge curves and contact interface changes of the working electrode during cycling. (a-d) The discharge/charge curves of TMCs on Cu foil at different cycles. (e) The schematic structure of the working electrode during cycling process. (f) Cross-sectional view EDS mapping of the fresh FeS₂ electrode, the electrode after 50 cycles and the electrode after 100 cycles at a current density of 1 A g⁻¹.

As the current collector, Cu foil is in contact with Fe and Na₂S in the active material, which means that Fe and Cu will undergo dynamic competitive reactions when the battery is charged back to 3 V, as shown in the following equations:



Copper sulfides have been reported to possess a unique displacement mechanism with lithium in LIBs that leads to much smaller overpotentials than are found in other conversion reactions, suggesting more facile kinetics during the reaction [19,20]. Cui's group has reported that the chemical diffusion coefficient of Cu in Cu₂S is much higher than that of other metal sulfides such as FeS₂ (approximately 10¹⁰ times higher) [20]. This implies that the active material FeS₂ will be replaced by copper sulfide through the above dynamic competition, which lead to the dramatic changes in the discharge/charge plateaus.

To analyze the component evolution of the active materials, energy-dispersive X-ray spectroscopy (EDS) elemental mapping was used to detect the distribution of Cu in the electrode before and after cycling. In the cross-sectional view in Fig. 1f, the original electrode shows an obvious demarcation between the active material (FeS₂) and Cu. After 50 cycles, it is difficult to distinguish between the active material (FeS₂) and Cu, which demonstrates that the Cu has diffused into the active material. After 100 cycles Cu has diffused throughout the entire active material. The other three samples also exhibit a similar trend in which Cu occupies the entire active material after 50 cycles (Fig. S2). These results indicate that Cu is truly involved in the electrochemical reaction of the electrode during cycling.

To reveal the influence of Cu on the electrochemical properties of TMC materials, control experiments were conducted using titanium (Ti) foil as the current collector in the assembled batteries.

Interestingly, when using the Ti current collector, the shape of the discharge/charge curves of the four samples is well maintained during cycling (Fig. 2a-d). The discharge/charge plateaus are just shortened along with the capacity fading without potential shift, which indicates the corresponding redox couples are not change [17]. Clearly, the cycling stability of the active materials supported on Cu is much better than that of those supported on Ti (Fig. 2e-h).

To gain further insight into the transformation mechanism, transmission electron microscopy (TEM) analysis was performed on the following TMCs supported on a Cu current collector: NiS₂ after 200 cycles and CoSe₂ after 50 cycles (as shown in Fig. 2i-o and Fig. S3). Remarkably, despite their different original morphologies, both samples exhibit similar morphologies in their fully charged states after cycling. In NiS₂ electrode, Cu is dominant in the active material according to the selected-area electron diffraction (SAED) pattern and EDS analysis, which indicates that almost all the NiS₂ transformed into copper sulfide species (CuS (JCPDS No. 06-0464), Cu_{1.9375}S (JCPDS No. 71-1383) and Cu₂S (JCPDS No. 72-1071)) after 200 cycles (Fig. 2i-o). The Cu_{2-x}S system exhibits rich crystal chemistry with a variety of closely related phases [20]. It is difficult to determine the exact phases of Cu_{2-x}S, owing to the similar diffraction patterns and the variable diffraction peak intensities of its nanocrystals [21,22]. Thus, we chose Cu_{1.9375}S (JCPDS No. 71-1383) and Cu₂S (JCPDS No. 72-1071) to refer to Cu_{2-x}S, according to the SAED pattern. For CoSe₂ electrode, it shows a small amount of residual CoSe₂ composited with a mass of Cu₂Se (JCPDS No. 76-0136) in the electrode, according to the SAED pattern and EDS analysis, which suggests that the Cu-driven conversion process is incomplete after 50 cycles (Fig. S3c, d and h). In brief, all of the results demonstrate that Cu is superior in this dynamic competition in the Cu-supported TMC-based batteries.

In-situ XRD technique was applied to explore the actual chemical/physical process for the component evolution of active materials (Fig. 3). The schematic structure of the *in-situ* XRD device is shown as Fig. 3a. One side of Be was coated by Cu via physical vapor

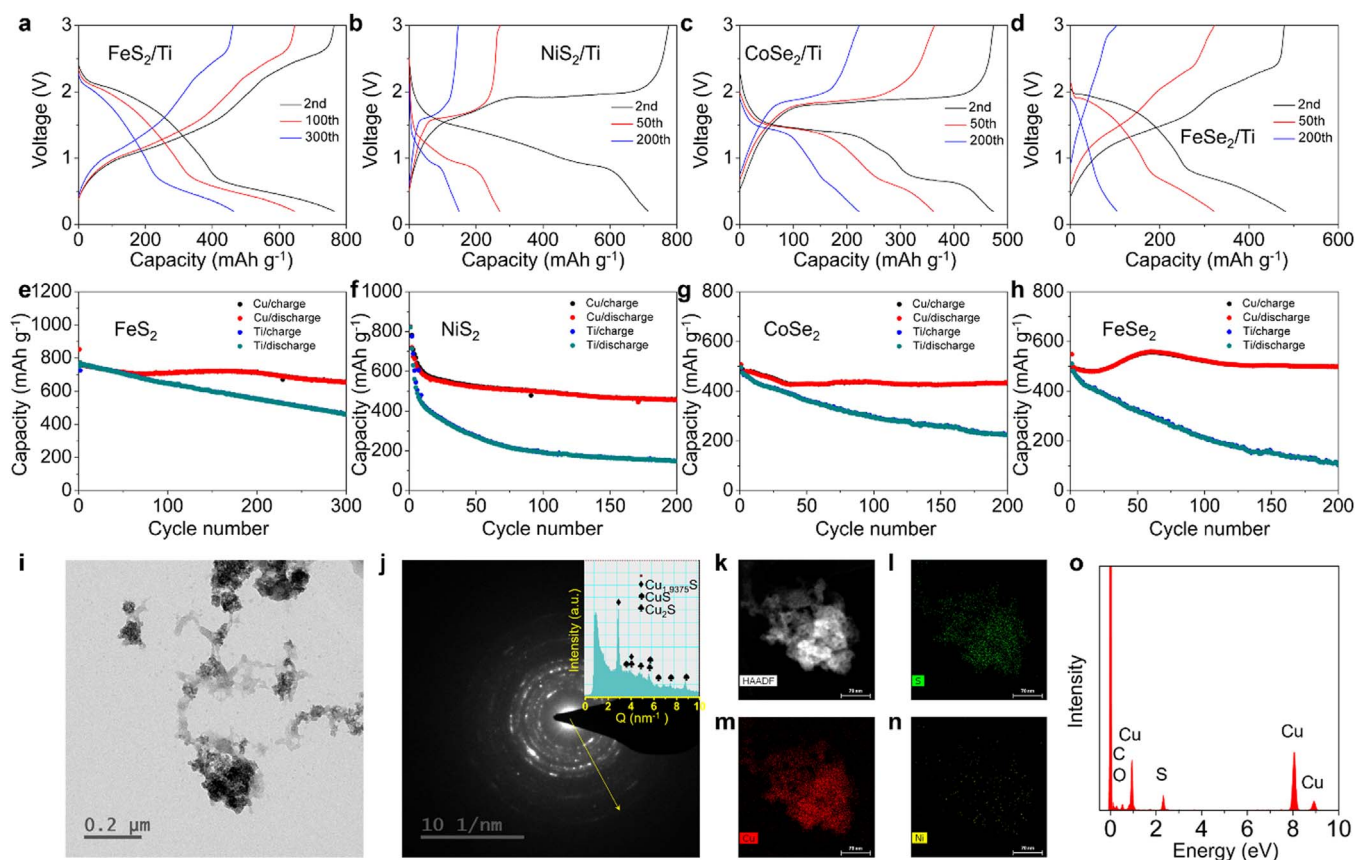


Fig. 2. The electrochemical performance of TMCs on Cu and Ti current collectors at 1 A g^{-1} and TEM studies of NiS_2 electrode after 200 cycles. (a–d) The discharge/charge curves of TMCs on Ti at different cycles. (e–h) The cycling performance of TMCs on different current collectors. (i) TEM image of the electrode shows the morphology of the active material and (inset) the corresponding HRTEM image shows a clear crystal lattice of Cu_2S and $\text{Cu}_{1.9375}\text{S}$. (j) The corresponding SAED pattern and integral curve of the yellow arrow determine the components of the active material. (k–o) EDS analysis reveals the element distribution of the electrode.

deposition (PVD) (the thickness of Cu is 200 nm), which was used as the current collector. Then the active material (FeSe_2) slurry was cast on the Cu and assembled the battery. Based on the XRD of the electrode (Fig. S4a), the 2θ were recorded from 30° to 45° , a range which can well reflect the changes of FeSe_2 and Cu. It demonstrates that a conversion reaction of FeSe_2 occurs with the potential below 1.00 V during the first discharge process, along with the disappearance of (101), (111) and (120) of FeSe_2 (Fig. 3b). This is attributed to the FeSe_2 crystals transform into a polycrystalline mixture of Na_2S and finely dispersed metallic iron which is hardly detected by XRD during the conversion reaction [20]. Interestingly, the Cu exhibits a periodical disappearance, which only occurs during the charge processes (Fig. 3b). This indicates that Cu would replace Fe to form the copper selenide during the charge processes along with the cycling, as we mentioned above. Fig. S4b shows the intensity of the (111) peak of Cu at full charge state of different cycles, which demonstrates that the 200 nm Cu layer has totally reacted after 4 cycles. The charge curve is also changed along with the consumption of Cu (Fig. 3b).

Based on the chemical and structural evolution features of typical TMCs, we identify that the stable capacity of TMCs on the Cu current collector is mainly attributed to the Cu. Although a number of cycles were achieved, all the capacity resulted from the copper sulfide or copper selenide species after the Cu-driven conversion process was completed. The whole process is defined as a Cu-driven conversion mechanism, as shown in Fig. 3c, and can be described as follows: (i) during the discharging process, TMCs react with Na^+ and are converted into transition metals and Na_2S or Na_2Se ; (ii) during the charging process, Cu reacts with Na_2S or Na_2Se to form copper sulfide or copper selenide species because of the faster diffusion rate of Cu ions in these species; and (iii) after several cycles, TMCs are completely converted

into copper sulfide or copper selenide species completely, which is indicated by the stabilization of the discharge/charge curves.

Inspired by the unique Cu-driven conversion mechanism, we designed a new type of sulfur-based battery, as illustrated in Fig. 4. Commercial sublimed sulfur was used as the cathode material. After ball-milling with the binder and acetylene black, the cathode material was then cast onto Cu foil to fabricate the electrode (Fig. 4a). The specific capacity values are calculated on the basis of the mass of sulfur. Fig. 4b reveals the cycling performance of the new sulfur-based battery between 0.2–3 V at a current density of 2 A g^{-1} . The battery delivers a stable capacity as high as 0.98 mAh cm^{-2} after 10 cycles, and even after 700 cycles the capacity still reaches $1.045 \text{ mAh cm}^{-2}$. The initial discharge capacity ($0.831 \text{ mAh cm}^{-2}$) is lower than that of later cycles owing to the slow reaction rate of sulfur and Na^+ , which results from the poor electrical conductivity of sulfur. During the first charging process, Na_2S is partly converted to copper sulfide species, which enhances the electrical conductivity of the entire active material owing to the good electrical conductivity of copper sulfides [22–24]. Then, the battery shows a greatly increased capacity ($1.004 \text{ mAh cm}^{-2}$) in the second discharging process, which is revealed in the discharge/charge curves of the first three cycles, as shown in Fig. S5. In addition, the discharge/charge curves also undergo a gradual stabilization process that is due to the accumulation of Cu in the active material (Fig. S5). We also evaluated the electrochemical performances of CuS and Cu_2S supported on Ti, as shown in Fig. S6. At the beginning of the cycling process for sulfur, the discharge/charge curves show a discharge plateau at $\sim 1.9 \text{ V}$ and a charge plateau at $\sim 2.1 \text{ V}$, which can be ascribed to the discharge/charge process of CuS (Supplementary Figs. 4 and 5c). Even more intriguing, after the discharge/charge curves stabilized, the discharge/charge curves of our new battery are consis-

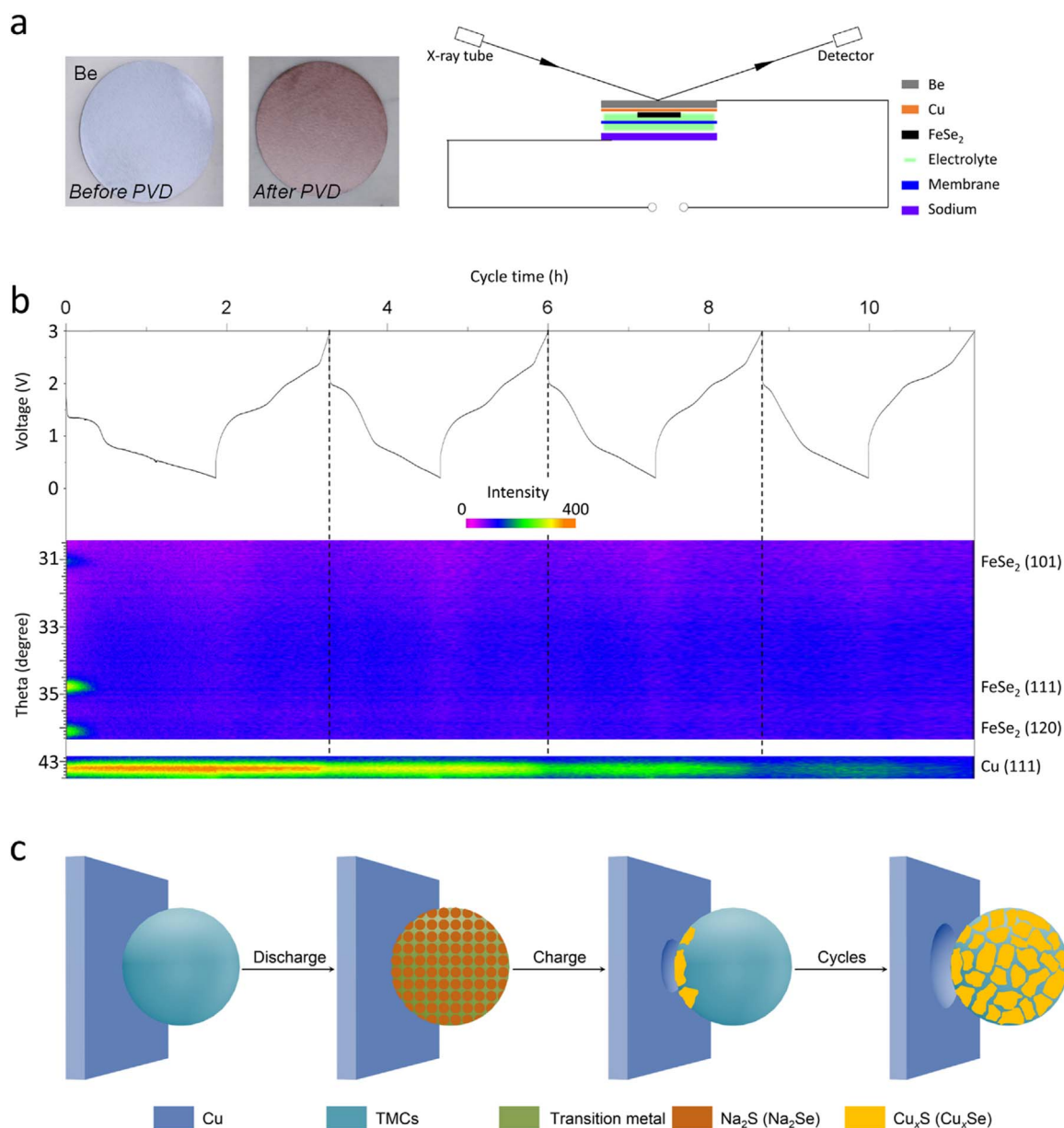


Fig. 3. *In-situ* XRD analysis and a schematic of the Cu-driven conversion mechanism for TMCs. (a) The illustration of the *in-situ* XRD instrument. (b) *In-situ* XRD patterns collected during galvanostatic charge/discharge of the FeSe₂ half-cell within 0.2–3 V. (c) A schematic of the Cu-driven conversion mechanism for TMCs during cycling.

tent with those of the pure Cu₂S cathode (Supplementary Figs. 4 and 5f). These results confirm the accumulation of Cu in the active material.

Furthermore, this new sulfur-based battery shows a superior rate capability, as shown in Fig. 4d. As the current densities gradually increase from 0.2 to 0.5, 1, 2, 5 and 10 A g⁻¹, the specific capacities of the battery change from 1.33 to 1.18, 1.13, 1.055, 0.9 and 0.59 mAh cm⁻², respectively. Even at an ultrahigh current density of 20 A g⁻¹, the capacity still remains at 0.33 mAh cm⁻². When the current density returns to 0.5 A g⁻¹, the capacity recovers to 1.160 mAh cm⁻². To evaluate the practicability of this battery, a high area loading (S: 5 mg cm⁻²) battery has been assembled. It shows good cycling stability at 0.2 A g⁻¹ (4.14 mAh cm⁻² after 30 cycles, as shown in Fig. S7a). But the high rate performance is inferior which is due to the poor kinetics result from the high loading (Fig. S7b). Detailed comparisons between this new type of battery and traditional RT sodium-sulfur batteries are listed in Table S1 [25,26]. This superior performance, achieved by such a simple and practical method, guarantees its real application in large-scale energy storage systems.

Moreover, a selenium-based battery was also assembled via the same method as shown in Fig. S8. This battery shows impressive cycle

stability after three cycles at 2 A g⁻¹. Similar to the sulfur-based battery, the selenium-based battery also presents a potential shift phenomenon. We should note that the Cu-driven conversion process in selenides is faster than that in sulfides (Fig. 4c, Fig. S5 and S8c). Similarly, the shape and plateau of the stabilized discharge/charge curves for the sodium-selenium battery are almost the same as that for FeSe₂ and CoSe₂ supported on Cu. The cyclic voltammetry (CV) curve of the selenium-based battery after 50 cycles exhibits three reduction peaks and two oxidation peaks, which is consistent with the previously reported CV curves of FeSe₂ and CoSe₂ [10,11]. These results demonstrate that our insight into the Cu-driven conversion mechanism can be extended to develop new selenide-based battery systems.

We should mention that the ether-based electrolyte greatly influences the Cu-driven conversion process for TMCs. When an ester-based electrolyte is used, the capacity of TMCs rapidly decays before the complete conversion of S to Cu_xS (Fig. S9a and b). Fig. S9 shows the electrochemical performance of sulfur supported on Ti. This system displays very fast capacity fading at a current density of 2 A g⁻¹ and exhibits discharge/charge plateaus corresponding to the 2Na⁺ + S + 2e⁻

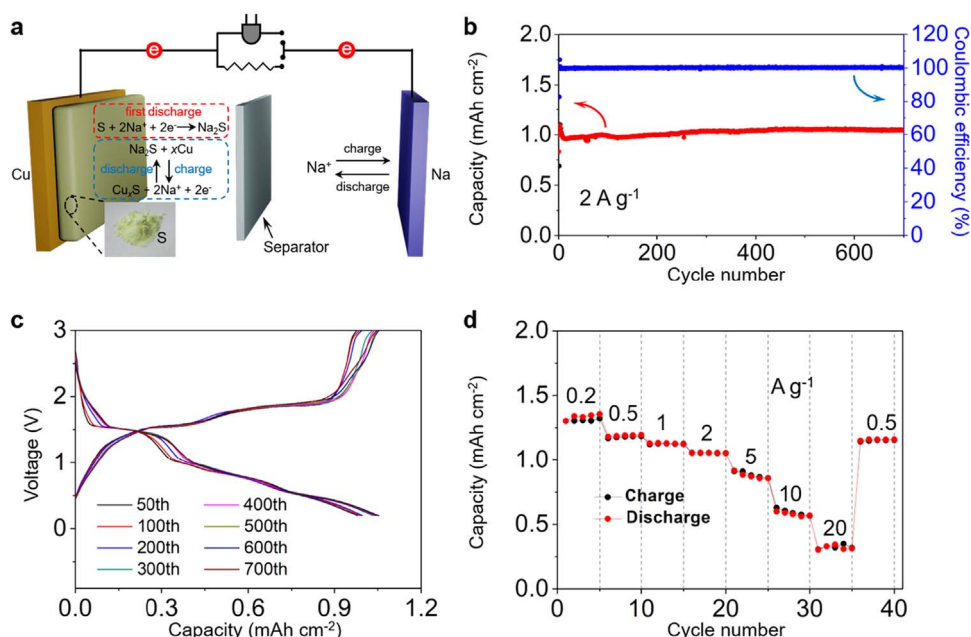


Fig. 4. A schematic and the electrochemical performance of our new type of sulfur-based battery. (a) A schematic of our new type of sulfur-based battery, which was prepared using commercial sublimed sulfur. (b, c) Cycling performance and corresponding discharge/charge curves of the battery at 2 A g^{-1} . (d) Rate performance of the battery. All the current densities are based on the mass of sulfur (1 mg cm^{-2}).

$\leftrightarrow \text{Na}_2\text{S}$ reaction (Fig. S9c and d) [27].

For this new sulfur-based battery system, it can be anticipated that Cu foil will become thinner owing to its dual role as current collector and active materials, and the amount of Cu consumption is correlated with the loading mass of sulfur. The weight of Cu current collector has been evaluated after different cycle, as shown in Fig. S10. The pristine Cu current collector is 13.52 mg (diameter is 14 mm , thickness is $10 \mu\text{m}$). The mass loading of S is 1 mg cm^{-2} . After 2 cycles, the weight decreases to 9.43 mg , and after 20 cycles, the weight stabilizes at around 8.5 mg (Fig. S10a and b). This result indicates that, in this sulfur-based batteries, the Cu-driven conversion process is drastic in the first few cycles and almost completed after 20 cycles. The actual active material loading is around 4.2 mg cm^{-2} after the Cu-driven conversion process completed (Fig. S10c). Moreover, the synchrotron HEXRD shows that, after 100 cycles, the active material has been converted to Cu_2S (Fig. S10d). Due to the superior reversibility of copper sulfides, the Cu foil will not be continually consumed after the Cu-driven conversion process completed. Even after 700 cycles, the Cu foil maintains good integrity, which means that the current collector function of Cu foil does not change (Fig. S10e).

Anode materials are typically supported on Cu current collectors for testing in LIBs and/or SIBs. Considering the above-described reaction mode of Cu and TMCs, we further examined the scenario in other anode systems in which Cu foil is involved. Vanadium oxides have been studied as active materials for rechargeable batteries for many years, both as anodes and as cathodes [28–30]. Interestingly, in $\text{Cu}_{2.33}\text{V}_4\text{O}_{11}$, the displacement reaction of Cu in the $[\text{V}_4\text{O}_{11}]_n$ layer has been reported to be electrochemically reversible [31]. This suggests that it is highly possible for Cu to insert into the layers of vanadium oxides in Cu-supported vanadium oxide electrodes, thus affecting their electrochemical performance. The insight that emerges from the unexpected Cu-driven conversion in our present anode systems can guide the rational choice of suitable current collectors. Meanwhile, this is an exciting new direction for the development of new energy storage systems that can take full advantage of Cu-driven conversion reactions.

4. Conclusion

We determined that the drastic potential shift of TMCs in SIBs is

caused by a Cu-driven conversion mechanism, which reveals the actual electrochemical reaction process of these materials. Based on the unique Cu-driven conversion mechanism, we developed a new sulfur-based battery system that possesses a superior electrochemical performance. This new type of sulfur-based battery shows great potential for large-scale energy storage systems. Furthermore, as the current collector, Cu participates in the reaction during cycling and thus influences the performance of many host materials. We proposed a new principle for choosing current collectors: an ideal current collector should be inert to both the electrolyte and the intermediate products of active materials during the cycling process. We believe that this work will be of great significance for future fundamental research into energy storage systems.

Acknowledgment

This work was supported by the National Key Research and Development Program of China (2016YFA0202603), the National Basic Research Program of China (2013CB934103), the Programme of Introducing Talents of Discipline to Universities (B17034), the National Natural Science Foundation of China (51521001 and 51602239), the National Natural Science Fund for Distinguished Young Scholars (51425204), the Hubei Provincial Natural Science Foundation of China (2016CFB267), and the Fundamental Research Funds for the Central Universities (WUT: 2016III001, 2016III003 and 2016IVA090). J.L. gratefully acknowledges support from the Assistant Secretary for Energy Efficiency and Renewable Energy, Office of Vehicle Technologies of the U.S. Department of Energy through the Advanced Battery Materials Research (BMR) Program (Battery500 Consortium). Argonne National Laboratory is operated for DOE Office of Science by UChicago Argonne, LLC, under Contract No. DE-AC02-06CH11357.

Competing financial interests

The authors declare no competing financial interests.

Appendix A. Supplementary material

Supplementary data associated with this article can be found in the online version at doi:10.1016/j.enstm.2018.07.002.

References

- [1] H. Tsai, W. Nie, J.-C. Blancon, C.C. Stoumpos, R. Asadpour, B. Harutyunyan, A.J. Neukirch, R. Verduzco, J.J. Crochet, S. Tretiak, *Nature* 536 (2016) 312–316.
- [2] A. Swarnkar, A.R. Marshall, E.M. Sanehira, B.D. Chernomordik, D.T. Moore, J.A. Christians, T. Chakrabarti, J.M. Luther, *Science* 354 (2016) 92–95.
- [3] X. Hu, W. Zhang, X. Liu, Y. Mei, Y. Huang, *Chem. Soc. Rev.* 44 (2015) 2376–2404.
- [4] D. Kundu, E. Talaie, V. Duffort, L.F. Nazar, *Angew. Chem. Int. Ed.* 54 (2015) 3431–3448.
- [5] S. Wei, S. Xu, A. Agrawal, S. Choudhury, Y. Lu, Z. Tu, L. Ma, L.A. Archer, *Nat. Commun.* 7 (2016) 11722.
- [6] Y. Sun, L. Zhao, H. Pan, X. Lu, L. Gu, Y.-S. Hu, H. Li, M. Armand, Y. Ikuhara, L. Chen, *Nat. Commun.* 4 (2013) 1870.
- [7] J. Sun, H.-W. Lee, M. Pasta, H. Yuan, G. Zheng, Y. Sun, Y. Li, Y. Cui, *Nat. Nanotechnol.* 10 (2015) 980.
- [8] Z. Hu, L. Wang, K. Zhang, J. Wang, F. Cheng, Z. Tao, J. Chen, *Angew. Chem.* 126 (2014) 13008–13012.
- [9] Z. Hu, Z. Zhu, F. Cheng, K. Zhang, J. Wang, C. Chen, J. Chen, *Energy Environ. Sci.* 8 (2015) 1309–1316.
- [10] K. Zhang, Z. Hu, X. Liu, Z. Tao, J. Chen, *Adv. Mater.* 27 (2015) 3305–3309.
- [11] K. Zhang, M. Park, L. Zhou, G.H. Lee, W. Li, Y.M. Kang, J. Chen, *Adv. Funct. Mater.* 26 (2016) 6728–6735.
- [12] M. Mao, C. Cui, M. Wu, M. Zhang, T. Gao, X. Fan, J. Chen, T. Wang, J. Ma, C. Wang, *Nano Energy* 45 (2018) 346–352.
- [13] C. Cui, Z. Wei, J. Xu, Y. Zhang, S. Liu, H. Liu, M. Mao, S. Wang, J. Ma, S. Dou, *Energy Storage Mater.* 15 (2018) 22–30.
- [14] J. Xu, J. Ma, Q. Fan, S. Guo, S. Dou, *Adv. Mater.* 29 (2017) 1606454.
- [15] S.-L. Yang, H.-B. Yao, M.-R. Gao, S.-H. Yu, *Crystengcomm* 11 (2009) 1383–1390.
- [16] W. Zhang, Z. Yang, J. Liu, Z. Hui, W. Yu, Y. Qian, G. Zhou, L. Yang, *Mater. Res. Bull.* 35 (2000) 2403–2408.
- [17] A.J. Bard, L.R. Faulkner, J. Leddy, C.G. Zoski, *Electrochemical Methods: Fundamentals and Applications*, Wiley, New York, 1980.
- [18] T. Kim, J. Choi, H. Ryu, G. Cho, K. Kim, J. Ahn, K. Cho, H. Ahn, *J. Power Sources* 174 (2007) 1275–1278.
- [19] B. Jache, B. Mogwitz, F. Klein, P. Adelhelm, *J. Power Sources* 247 (2014) 703–711.
- [20] M.T. McDowell, Z. Lu, K.J. Koski, J.H. Yu, G. Zheng, Y. Cui, *Nano Lett.* 15 (2015) 1264–1271.
- [21] M. Lotfipour, T. Machani, D.P. Rossi, K.E. Plass, *Chem. Mater.* 23 (2011) 3032–3038.
- [22] Y. Zhao, H. Pan, Y. Lou, X. Qiu, J. Zhu, C. Burda, *J. Am. Chem. Soc.* 131 (2009) 4253–4261.
- [23] L.-W. Wang, *Phys. Rev. Lett.* 108 (2012) 085703.
- [24] H.T. Evans, *Z. für Krist. - Cryst. Mater.* 150 (1979) 299–320.
- [25] X. Yu, A. Manthiram, *ChemElectroChem* 1 (2014) 1275–1280.
- [26] I. Bauer, M. Kohl, H. Althues, S. Kaskel, *Chem. Commun.* 50 (2014) 3208–3210.
- [27] A. Manthiram, X. Yu, *Small* 11 (2015) 2108–2114.
- [28] Q. Li, Q. Wei, Q. Wang, W. Luo, Q. An, Y. Xu, C. Niu, C. Tang, L. Mai, *J. Mater. Chem. A* 3 (2015) 18839–18842.
- [29] Q. Wei, Z. Jiang, S. Tan, Q. Li, L. Huang, M. Yan, L. Zhou, Q. An, L. Mai, *ACS Appl. Mater. Inter.* 7 (2015), 2015, pp. 18211–18217.
- [30] L. Mai, Q. Wei, Q. An, X. Tian, Y. Zhao, X. Xu, L. Xu, L. Chang, Q. Zhang, *Adv. Mater.* 25 (2013) 2969–2973.
- [31] M. Morcrette, P. Rozier, L. Dupont, E. Mugnier, L. Sannier, J. Galy, J.-M. Tarascon, *Nat. Mater.* 2 (2003) 755–761.